Title

Photoelectron Spectroscopy and Electronic Structure of Clusters of the Group V Elements. I. Dimers

Journal

Journal of chemical physics, 93(9)

Authors

Wang, L.-S.
Lee, Yuan T.
Shirley, D.A.
et al.

Publication Date

1990-06-01

LBL-28871
Preprint

Lawrence Berkeley Laboratory
UNIVERSITY OF CALIFORNIA

Materials & Chemical Sciences Division

Submitted to Journal of Chemical Physics

Photoelectron Spectroscopy and Electronic Structure of Clusters of the Group V Elements. I. Dimers

L.-S. Wang, Y.T. Lee, D.A. Shirley,
K. Balasubramanian, and P. Feng

June 1990

Prepared for the U.S. Department of Energy under Contract Number DE-AC03-76SF00098.

DISCLAIMER

LBL-28871

Photoelectron Spectroscopy and Electronic Structure of Clusters of the Group V Elements. I. Dimers

L.-S. Wang, Y.T. Lee, and D.A. Shirley
Department of Chemistry
University of California
and
Materials and Chemical Sciences Division
Lawrence Berkeley Laboratory
University of California
Berkeley, CA 94720

and

K. Balasubramanian* and P. Feng
Department of Chemistry
Arizona State University
Tempe, AZ 85287

*Camille and Henry Dreyfus Teacher-Scholar.

This work was supported by the Director, Office of Energy Research, Office of Basic Energy Sciences, Chemical Sciences Division of the U.S. Department of Energy under Contract No. DE-AC03-76SF00098, by the National Science Foundation through Grant CHE8818869, and by the Alexander von Humboldt Foundation through a Senior Scientist Award to DAS.

Abstract

The HeI (584Å) high resolution photoelectron spectra of As_2^+, Sb_2^+, and Bi_2^+ have been obtained with a high temperature molecular beam source. A pure As_2 beam was produced by evaporating Cu_3As. Sb_2 was generated as a mixture with the atoms and tetramers by evaporating the pure element, while Bi_2 was generated as a mixture with only the atoms from the pure element. Vibrational structure was well resolved for the As_2^+ spectrum. Spectroscopic constants were derived and reported for the related ionic states. In addition, we have carried out relativistic complete active space self-consistent field followed by multi-reference single + double configuration interaction calculations on these dimers both for the neutral ground states and the related ionic states. The agreements between the calculated and experimentally derived spectroscopic constants were fairly good, although the calculations tended to underestimate consistently the strength of the bonding in these heavy homonuclear diatomics.

I. Introduction

The study of metal clusters has drawn great attention recently because of their importance in many disciplines, including surface sciences, catalysis, inorganic chemistry, materials sciences, etc. The intermediate nature of these species gives rise to many unique chemical and physical properties, such as enhanced chemical reactivity and quantum size effects. A large body of literature including numerous review articles[1] has been devoted to various aspects of this subject. Of particular interest, both for their technological and fundamental importances, are clusters composed of semiconductor elements. Indeed, a number of investigations have focussed on Si clusters[2] and other semiconductor clusters.[3] The group V elements, especially P, As, and Sb, are also important in relation to semiconductor materials. Nevertheless, there have been few studies on their clusters.

One central question in cluster research is the evolution of electronic properties as a function of cluster size. For small clusters, molecular electronic spectroscopic techniques should be well suited for this study. In particular, photoelectron spectroscopy (PES) should be a powerful technique, because it probes directly the electronic energy levels of matter.[4] However, one difficulty in applying PES to cluster species is the need for size-selectivity. Consequently, much effort has been focused on photodetachment of negatively-charged clusters.[5] Only recently have studies employing PES been carried out on size-selected neutral clusters.[6]

We are interested in high resolution PES of small neutral clusters. A high temperature molecular beam source[7,8] has been built to facilitate studies on small neutral clusters and high temperature species. Besides being important semiconductor doping materials, the group V elements are well suited for our study because they provide an easy solution for the size-selectivity. Vapor phases of these elements[9] are mainly composed of tetramer species for P and As; atoms, dimers, and tetramers for Sb; and dimers and atomic species for Bi. Diatomic P and As can be produced by pyrolyzing the tetramers, or by

evaporating an appropriate alloy of these elements. In the current paper, we present our study on high resolution PES of As_2, Sb_2, and Bi_2. In addition, we have carried out relativistic quantum chemical calculations in conjunction with the experimental study. The study on the tetramer species will be reported in a subsequent paper.

Lower resolution HeI (584 Å) PE spectra of As_2[10], Sb_2[11], and Bi_2[12] have been reported. However, no vibrational resolution was achieved and little is known about the cationic states of these diatomics. Theoretically, the neutral As_2,[13] Sb_2,[14a] and Bi_2[14b] have been studied. The theoretical calculation on Bi_2 was restricted only to the ground state while potential energy curves of a number of electronic states of As_2 and Sb_2 have been obtained before.[13,14a] However, there have been no theoretical calculations on the ionic states of these dimers. We have obtained high resolution PE spectra for the three molecules. Vibrational structure was completely resolved for the As_2^+ spectrum. The spectra of Sb_2 and Sb_4 overlapped with each other, which prevented us from resolving any vibrational structure for the Sb_2 spectrum. The Bi_2 molecule has a very small vibrational frequency. Nevertheless, we were still able to resolve partial vibrational structure in the $^2\Sigma_g^+$ band. Franck-Condon factor (FCF) calculations were carried out to analyze the ionic states, allowing us to obtain important spectroscopic constants. In addition, we carried out relativistic quantum chemical calculations to compare with the experimental results.

This paper is organized as follows. In Section II, we briefly present the experimental procedure, and in Section III the method of the theoretical calculations. The results and data analysis are given in Section IV. Discussions of the results and comparisons with the theoretical calculations are presented in Section V and the conclusions appear in Section VI.

II Experimental

The high temperature molecular beam source used in the current experiments has been described in detail previously.[7,8] The experimental conditions relevant to the current experiments are given collectively in Table 1. The arsenic dimer was produced by evaporating a Cu_3As compound at a temperature of about 1400 K, as it was shown that this would yield pure As_2 species.[10b] We also used a quadrupole mass spectrometer to confirm this, since all our evaporations were monitored by the quadrupole mass spectrometer. A pure antimony sample was used to produce Sb_2. At the experimental temperature given in Table 1, the vapor of antimony contained three species: atoms, dimers, and tetramers. As a result, the PE spectrum was a mixture of the three. Also a pure bismuth sample was used for the Bi_2 experiment and its vapor was composed of both atoms and dimers. Fortunately, the atomic contributions to the PE spectrum can easily be subtracted, and a pure dimer spectrum can still be obtained. All samples (99% purity) were purchased from CERAC and used directly.

The details of the PE spectrometer have also been described previously.[15] Argon and xenon were used as calibration gases. The energy resolution was 12 meV, as measured with the $Ar^+ {}^2P_{3/2}$ PE peak. To avoid drift of the energy scale under the high temperature conditions, we kept each PE scan under one hour. Multiple scans were taken and added together to increase counting statistics. The effective energy resolution on the final spectrum was about 15 meV.

III. Method of Theoretical Calculations

We employed a (4s4p4d) valence Gaussian basis set for the As, Sb, and Bi atoms in our calculations. The outer $(n-1)d^{10}ns^2np^3$ shell (15 electrons) were explicitly retained in the calculations. The rest of the core electrons were replaced by a relativistic effective

core potential (RECP) generated by LaJohn et al.[16] The basis sets used are given in Table 2.

We carried out multi-configuration self-consistent field (MCSCF) calculations to generate the orbitals for configuration interaction (CI) calculations, using the complete active space MCSCF (CASSCF) method, in which valence electrons were distributed in all possible ways among a chosen set of orbitals referred to as the internal space of orbitals. For the present molecules and ions, we included all orbitals in the internal space which correlated into the 5s and 5p atomic orbitals at infinite separations. In the $D_{\infty h}$ symmetry, these orbitals are $1\sigma_g$, $1\sigma_u$, $2\sigma_g$, $2\sigma_u$, $1\pi_u$, and $1\pi_g$ orbitals. The CASSCF and CI calculations were actually accomplished in the D_{2h} point group. All the molecules and ions were oriented along the z axis which was also chosen as the C_2 axis. The σ_{xz} and σ_{yz} were the planes of symmetry. In this orientation, the active space consisted of two A_g, two B_{3u}, one B_{1u}, one B_{1g}, one B_{2u}, one B_{2g}, one B_{3g}, and one A_u orbitals. The 9 valence electrons of the ions or the 10 valence electrons of the neutral molecules, which we refer to as the active electrons, were distributed in all possible ways among the internal set of orbitals.

The CI calculations were done after the MCSCF calculations. They were carried out using the CASSCF, followed by a multi-reference singles + doubles CI (MRSDCI) method for the ground states of the molecules and the two lowest-lying electronic states of the ions, accessed in the experiments. The MRSDCI calculations included single and double excitations from a set of chosen reference configurations which had coefficient $\geq$ 0.07 in the CASSCF. The dimensions of the CASSCF calculations were between 176 and 308 in the D_{2h} point group, while the MRSDCI calculations included between 180,426 and 199,512 configurations.

We also conducted relativistic CI (RCI) calculations for the spin-orbit effects in the $^2\Pi_u$ ionic states and the neutral ground states. The RCI calculations were done using the natural orbitals obtained from a CASSCF/CI calculation with the Gaussian basis sets. The

RCI calculations included all possible states with the same Ω symmetry, and single and double excitations from the reference configurations. The spin-orbit integrals, obtained using the differences of (l +1/2) and (l -1/2) RECPs and the Gaussian basis sets in Table 2, were transformed over the natural orbitals, obtained from CASSCF/CI calculations done without the spin-orbit term. The transformed integrals were then added to the transformed one-electron matrix elements at the RCI stage. Another set of calculations with the same configurations without the spin-orbit integrals were performed. The difference between the two were applied to the CASSCF/MRSDCI results which did not contain the spin-orbit term.

The CASSCF/MRSDCI calculations were accomplished with a modified version[17] of the ALCHEMY II codes[18] to include the RECPs. The RCI calculations were carried out with the method described in Ref. 19. The spin-orbit integrals over Gaussian basis sets were done using a Pitzer's modified version of ARGOS.[20]

IV. Results and data analysis

The group V elements have ns^2np^3 atomic valence electron configurations, where the core electrons are not shown. From the molecular orbital (MO) theory, the homonuclear diatomic molecules of these elements have the following valence electronic configurations: $(\sigma_g ns)^2 (\sigma_u ns)^2 (\sigma_g np)^2 (\pi_u np)^4$, where (nl) denotes the dominant components of the MOs.

The PE spectra are shown in Figs. 1-3 for As_2^+, Sb_2^+, and Bi_2^+, respectively. Only the ionizations of the two MOs derived from the np atomic orbitals were observed in our experiments. The atomic ionization cross sections of the ns orbitals are two to three orders of magnitude smaller than that of the np orbitals at the HeI photon energy (21.218 eV).[21] Thus, it is not surprising that the ionizations of the ($\sigma_g$ns) and ($\sigma_u$ns) orbitals were not observed. Vibrational structure was well resolved for As_2^+, with the two spin-orbit

split $^2\Pi_u$ bands partially overlapped. The $^2\Sigma_g^+$ band is very sharp, with little vibrational structure.

As mentioned in Section II, the antimony spectrum is a mixture of Sb^+, Sb_2^+, and Sb_4^+. Fig. 2 shows the $Sb_2^+ + Sb_4^+$ $[(2t_2)^{-1}]$ portion of the spectrum with the three atomic lines subtracted. This could be done because the atomic line shape was known from our calibrations with the rare gases, which were best fitted with Voigt functions. Thus, a Voigt function was fitted to each Sb^+ peak , and then subtracted from the spectrum. The subtracted Sb^+ peaks are also plotted in Fig. 2 at their actual peak positions and with their actual line shapes. What is left is still a mixture of the Sb_2^+ and Sb_4^+ $[(2t_2)^{-1}]$ spectra, with the Sb_2^+ spectrum sitting on the $(2t_2)^{-1}$ bands of Sb_4^+. The $^2\Sigma_g^+$ band of Sb_2^+ is sharp and easily recognized. Unfortunately, the $^2\Pi_{u1/2}$ and $^2\Pi_{u3/2}$ bands are overlapped heavily with the Sb_4^+ $(2t_2)^{-1}$ bands and cannot be separated and assigned.

The bismuth vapor contained both Bi and Bi_2. At our experimental temperature, there was about 35% Bi_2 in the vapor.[9] The spectrum shown in Fig. 3 is the pure Bi_2^+ spectrum after the atomic lines were subtracted. The positions of the three atomic peaks are indicated in Fig. 3. We did not plot them in the figure, because they had much higher intensity than the pure Bi_2^+ spectrum. The subtraction procedure was the same as with the Sb^+ lines in Fig. 2. The energy range between about 8 to 8.6 eV in Fig. 3 was not scanned to save running time, because it was known that there were no peaks in this energy range.[12] The ground state vibrational frequency[22] of Bi_2 is 172.71 cm^{-1}, and it is anticipated to be even smaller in the ion. The vibrational population of Bi_2 in the molecular beam was expected to be high because of its small vibrational frequency and the ineffectiveness of the vibrational relaxation in the supersonic expansion. Both of these factors contributed to the lack of vibrational resolution in the Bi_2^+ spectrum. In fact, a hot-band transition was observed on the low energy side of the $^2\Sigma_g^+$ band, which was useful for an evaluation of the vibrational temperature.

To analyze the spectra , we carried out FCF simulations for the As_2^+ and Bi_2^+ spectra. The calculations were done in the same way as described before.[23-25] Basically, a Morse oscillator was employed and was expanded as a power series in $(r-r_e)$, where r_e is the equilibrium bond length. The $(r - r_e)^3$ and $(r - r_e)^4$ terms were taken as perturbation corrections to the harmonic oscillator Hamiltonian. A few kinds of valuable information can be obtained from such calculations, e.g., the vibrational temperature of molecules in a beam, the vibrational frequency and equilibrium bond length of a particular ionic state, refined values of adiabatic IPs in cases where there are band overlappings or strong hot band transitions.

Fig. 4 shows a comparison of the calculated spectrum with the experimental one for the $^2\Sigma_g^+$ state of As_2^+. A vibrational temperature of 600K was used in this calculation. We obtained a vibrational frequency of 390(6) cm^{-1} and an equilibrium bond length of 2.115(5) Å. However, the vibrational analyses of the $^2\Pi_{u3/2}$ and $^2\Pi_{u1/2}$ bands were complicated by two factors, the hot band transitions and the heavy overlapping of the two bands. Both factors made it difficult to determine the adiabatic IPs and were responsible for the fact that the $^2\Pi_{u3/2}$ band appears to have larger vibrational spacings than the $^2\Pi_{u1/2}$ band. Figs. 5 and 6 illustrate the best fits for these two bands with the vibrational temperature of 600K, derived above from the simulation of the $^2\Sigma_g^+$ band. From these fits, adiabatic IPs of 9.636 eV and 9.810 eV were derived for the $^2\Pi_{u3/2}$ and $^2\Pi_{u1/2}$ states, respectively. It can be seen that the hot band transitions were very serious, and in the case of the $^2\Pi_{u1/2}$ band, they extanted well into the $^2\Pi_{u3/2}$ band and superimposed on it. Thus, the FCF calculations were really helpful in analyzing these two spin-orbit bands. The vibrational frequencies and equilibrium bond lengths derived for the $^2\Pi_{u3/2}$ and $^2\Pi_{u1/2}$ states are 385(8) cm^{-1} and 380(5) cm^{-1}, and 2.230(8) Å and 2.235(8) Å, respectively.

FCF simulations of the $^2\Sigma_g^+$ state of Sb_2^+ allowed us to derive a vibrational frequency of 235(10) cm^{-1} and an equilibrium bond length of 2.37(1) Å. However, the

overlapping of the Sb_2^+ and Sb_4^+ spectra prevented us from doing similar FCF simulations for the spin-orbit split $^2\Pi_{u3/2}$ and $^2\Pi_{u1/2}$ bands of Sb_2^+.

Fig. 7 shows a FCF calculation for the $^2\Sigma_g^+$ state of Bi_2^+ in comparison with the experimental spectrum. Although the vibrational frequency here is very small, discernible vibrational structure was still resolved, allowing us to derive quantitative spectroscopic constants. The vibrational temperature for Bi_2 was estimated to be about 400(50) K, which still caused considerable hot band transitions, as can be seen in Fig. 7, where the adiabatic IP is at 9.307 eV. From the simulation, we obtained a vibrational frequency of 150(8) cm^{-1} and an equilibrium bond length of 2.705(5) Å for the $^2\Sigma_g^+$ state of Bi_2^+. Since there was no vibrational structure resolved for the two spin-orbit split $^2\Pi_{u3/2}$ and $^2\Pi_{u1/2}$ bands of Bi_2^+, it was more difficult to do quantitative simulations. Basically, with the vibrational temperature fixed at 400(50) K, we changed the adiabatic IPs, the equilibrium bond lengths, and the vibrational frequencies until we achieved best fits in band shapes by visual inspections. Therefore, the results from the calculations can only be regarded as estimates. All the derived spectroscopic constants are tabulated in Tables 3-5 together with the theoretical calculations for As_2^+, Sb_2^+ and Bi_2^+, respectively.

From the measured IPs, the dissociation energy (D_e) of the ground ionic state can be calculated from the following:

$$D_e (M_2^+) = D_e (M_2) + IP (M) - IP (M_2) \qquad (1)$$

where $D_e (M_2)$ is the dissociation energy of the neutral ground state, IP (M) is the IP of the atom, IP (M_2) is the adiabatic IP of the molecule measured in this experiment, as given in Tables 3-5. The calculated ground state D_es from Eq. (1) are also given in Tables 3-5 for each ion.

V. Discussion

In Tables 3-5, the experimentally derived spectroscopic constants are compared with the theoretical calculations. The CASSCF/CI/RCI potential energy curves for the related photoionizations were also calculated and are shown in Figs. 8 and 9 for As_2^+ and Sb_2^+, respectively. The potential energy curves of Bi_2^+ were obtained using the less accurate CASSCF/RCI method, as shown in Fig. 9. Calculations both with and without the spin-orbit effects were carried out. The spectroscopic constants without including the spin-orbit effect for the $^2\Pi_u$ states are also given in Tables 3-5 for each case. It is seen that the spin-orbit effect gets increasingly more important from As_2^+ to Bi_2^+. The D_e values for the $^2\Pi_u$ states were calculated only for the cases without including the spin-orbit effect, because the calculations with the spin-orbit effect demanded to calculate the potential energies up to infinite atomic separations and were difficult to be carried out in a size-consistent manner. Thus, for the potential energy curves of Bi_2^+, Bi_2, and Sb_2^+, we only calculated the parts around the equilibrium nuclear separations with the spin-orbit effect, as seen in Figs. 8 and 9. Overall, the agreements between the experimental and theoretical results are fairly good, considering the complexity of the systems at hand. In general, the calculations tend to underestimate the strength of the chemical bonding in these homonuclear diatomics, because they give consistently lower values for the D_es, IPs, and ω_es, and larger values for the R_es.

The spectroscopic constants of the neutral molecules[26] are also shown in Tables 3-5 for comparisons. According to the simple valence MO picture, the π_u orbital is a bonding orbital. The removal of an electron from this orbital should weaken the bonding. This is manifested as lengthening of the bond lengths and decreasing of the vibrational frequencies in the cationic states, as seen in Table 3-5. However, such changes are smaller in magnitude upon removing a σ_g electron. Thus, relatively speaking, the π_u orbital is more strongly bound than the σ_g orbital.

It is interesting to note that the two spin-orbit states, $^2\Pi_{u1/2}$ and $^2\Pi_{u3/2}$, have slightly different experimental vibrational frequencies. The theoretical calculations with the spin-orbit effect yielded identical ω_es for the two states. Hence, it appears that it may not be due to the spin-orbit effect. A similar case has been observed for Br_2^+, where two very different vibrational frequencies were observed for the two spin-orbit states of the $A^2\Pi_u$ bands, which was explained by a strong spin-orbit contamination of the $A^2\Pi_{u1/2}$ state from a nearby $^4\Sigma_{u1/2}^-$ state.[27] We did a similar calculation for As_2^+ and found that the closest higher-lying state which can interact with the $^2\Pi_{u1/2}$ state is a $^4\Sigma_u^-$ term, some 2.6 eV above the $^2\Pi_{u1/2}$ state. Its spectroscopic properties were calculated and are also given in Table 3. Because of the large energy separation, it is not surprising that we did not find a significant enough spin-orbit mixing of the $^2\Pi_{u1/2}$ state with the $^4\Sigma_u^-$ term. On the other hand, because of the spin-orbit splitting, the $^2\Pi_{u3/2}$ state should have a slightly deeper potential well than the $^2\Pi_{u1/2}$ state. Hence, they are expected to have slightly different spectroscopic constants. This difference probably is too small to be reproduced theoretically. It is noticed from Table 3 that the calculated and experimental ω_es for the $^2\Sigma_g^+$ state agree excellently, while the calculated ω_es for the $^2\Pi_u$ states are much smaller than the experimental ones.

The increasing importance of the spin-orbit effects from As_2 to Bi_2 are illustrated more clearly in Figs. 8-10, where potential energy curves both with and without the spin-orbit effects are plotted. The effect is too small for As_2 on the energy scale used in Fig. 8. It is interesting to note that the $^2\Pi_{u1/2}$ and the $^2\Sigma_g^+$ curves cross with each other, because they have different g and u symmetries. Our earlier study on the group IV-VI diatomics[25] have shown that such crossings induce avoided curve-crossings, because there are no g and u symmetry constraints in those systems.

Interestingly, a recent resonance enhanced photodissociation spectroscopy study of Bi_2^+ [28] suggested to have observed transitions from the ground $^2\Pi_{u3/2}$ state to the $^2\Sigma_g^+$ state in Bi_2^+. A vibrational frequency of 179.6 cm^{-1} was derived for the ground state, and

a value of 143.4 cm^{-1} was assigned to the excited state. The later is in good agreement with the value of 150(8) cm^{-1} derived in the current work for the $^2\Sigma_g^+$ state of Bi_2^+, while the value of 179.6 cm^{-1} for the proposed $^2\Pi_{u3/2}$ state seems to be too large. The estimated vibrational frequency for the $^2\Pi_{u3/2}$ state in the current work is about 140 cm^{-1}, as given in Table 5. Furthermore, the value of 179.6 cm^{-1} is even larger than the vibrational frequency of the neutral ground state and is in direct conflict with the fact that the $^2\Pi_{u3/2}$ state is less bound than the neutral ground state. Therefore, the observed resonance enhanced photodissociation spectrum of Bi_2^+ may need to be reanalyzed.[29]

VI. Conclusions

We have obtained the high resolution photoelectron spectra for As_2^+, Sb_2^+, and Bi_2^+. Vibrational structure was well resolved for As_2^+. Franck-Condon factors analyses allowed us to derive important spectroscopic constants for the cations. Relativistic CASSCF/MRSDCI/RCI calculations were performed for the related neutral and ionic states to compare with the experimental results, and the agreements were fairly good with such complicated systems.

Acknowledgment

DAS thanks the Alexander von Humboldt Foundation for support through a Senior Scientist Award, and Professors G. Kaindl and E. Mattias for their hospitality during his stay in FB Physik, FU Berlin. The experimental work at Berkeley was supported by the Director, Office of Energy Research, Office of Basic Energy Sciences, Chemical Sciences Division of the U.S. Department of Energy under Contract No. DE-AC03-76SF00098, while the theoretical work at Arizona was funded by the National Science Foundation through grant CHE8818869.

References

1. See for example, (a) T.P. Martin, *Phys. Rep.* **95**, 167 (1983); (b) J.C. Phillips, *Chem. Rev.* **86**, 619 (1986); (c) M.D. Morse, *Chem. Rev.* **86**, 1049 (1986); (d) W. P. Halperin, *Rev. Modern Phys.* **58**, 533 (1986); (e) D.R. Salahub, *Adv. Chem. Phys.* **69**, 447 (1987); (f) M.M. Kappes, *Chem. Rev.* **88**, 369 (1988); (g) K. Balasubramanian, *Chem. Rev.* **89**, 1801 (1989); **90**, 93 (1990).
2. See for example, (a) K. Raghavachari, *J. Chem. Phys.* **83**, 3520 (1985); (b) L.A. Bloomfield, R.R. Freeman, and W.L. Brown, *Phys. Rev. Lett.* **54**, 2246 (1985); (c) J.C. Phillips, *J. Chem. Phys.* **83**, 3330 (1985); (d) D. Tomanek and M.A. Schluter, *Phys. Rev.* **B36**, 1208 (1987); (e) K. Balasubramanian, *Chem. Phys. Lett.* **135**, 283 (1987); (f) J.L. Elkind, J.M. Alford, F.D. Weiss, R.T. Laaksonen, and R.E. Smalley, *J. Chem. Phys.* **87**, 2397 (1987); (g) M.L. Mandich, W.D. Reents, Jr., and M.F. Jarrold, *J. Chem. Phys.* **88**, 1703 (1988); (h) J. C. Phillips, *J. Chem. Phys.* **88**, 2090 (1988).
3. See for example, (a) T.P. Martin and H. Schaber, *J. Chem. Phys.* **83**, 855 (1985); (b) S.C. O'Brien, Y. Lin, Q. Zhang, J.R. Heath, F.K. Tittel, R.F. Curl, and R.E. Smalley, *J. Chem. Phys.* **84**, 4074 (1986); (c) K. Balasubramanian, *J. Chem. Phys.* **86**, 3410 (1987); (d) J.C. Phillips, *J. Chem. Phys.* **87**, 1712 (1987); (e) W. Schulze, B. Winter, and I. Goldenfeld, J. *Chem. Phys.* **87**, 2402 (1987); (f) L.B. Knight, Jr. and J.T. Petty, *J. Chem. Phys.* **88**, 481 (1988).
4. See for example, J.W. Rabalais, *Principles of Ultraviolet Photoelectron Spectroscopy* (Wiley, New York, 1977).
5. (a) O. Cheshnovsky, S.H. Yang, C.C. Pettiette, M.J. Craycraft, and R.E. Smalley, *Rev. Sci. Instrum.* **58**, 2131 (1987); (b) K. M. Ervin, J. Ho, and W.C. Lineberger, *J. Chem. Phys.* **89**, 4514 (1988).
6. K. Rademann, *Ber. Bunsenges. Phys. Chem.* **93**, 653 (1989).

7. (a) L.S. Wang, B. Niu, Y.T. Lee, and D.A. Shirley, *Chem. Phys. Lett.* **158**, 297 (1989); (b) L.S. Wang, B. Niu, Y.T. Lee, D.A. Shirley, and K. Balasubramanian, *J. Chem. Phys.* **92**, 899 (1990).

8. (a) L.S. Wang, **Ph.D. Thesis**, University of California, Berkeley, 1990, LBL-28606; (b) L.S. Wang, J.E. Reutt-Robey, B. Niu, Y.T. Lee, and D.A. Shirley, *J. Electron Spectrosc. Relat. Phenom.* **51**, 513 (1990).

9. A.N. Nesmeyanov, R. Gary (ed.), *Vapor Pressure of the Chemical Elements* (Elsevier, Amsterdam, 1957).

10. (a) S. Elbel, H.T. Dieck, H. Walther, and J. Krizek, *Inorg. Chim. Acta* **53**, L101 (1981); (b) J.M. Dyke, S. Elbel, A. Morris, and J.C.H. Stevens, *J.Chem. Soc. Faraday Trans.* II **82**, 637 (1986).

11. J.M. Dyke, A. Morris, and J.C.H. Stevens, *Chem. Phys.* **102**, 29 (1986).

12. S. Suzer, S.T. Lee, and D.A. Shirley, *J. Chem. Phys.* **65**, 412 (1976).

13. (a) J. Andzelm, N. Russo, and D.R. Salahub, *Chem. Phys. Lett.* **142**, 169 (1987); (b) K. Balasubramanian, *J. Mol. Spectrosc.* **121**, 465 (1987).

14. (a) K. Balasubramanian and J.Q. Li, *J. Mol. Spectrosc.* **135**, 169 (1989); (b) P.A. Christiansen, *Chem. Phys. Lett.* **109**, 145 (1984).

15. J.E. Pollard, D.J. Trevor, Y.T. Lee, and D.A. Shirley, *Rev. Sci. Instrum.* **52**, 1837 (1981).

16. L.A. LaJohn, P.A. Christiansen, R.B. Ross, T. Atashroo, and W.C. Ermler, *J. Chem. Phys.* **87**, 2812 (1987).

17. K. Balasubramanian, *Chem. Phys. Lett.* **127**, 585 (1986).

18. The major authors of the ALCHEMY II codes are B. Liu, B. Lengsfield, and M. Yoshiminie.

19. K. Balasubramanian, *J. Chem. Phys.* **89**, 5731 (1988).

20. R.M. Pither and N.W. Winter, *J. Phys. Chem.* **92**, 3061 (1988).

21. J.J. Yeh and I. Lindau, *Atomic Data and Nuclear Data Tables* **32**, 1 (1985).

22. K. Manzel, U. Engelhardt, H. Abe, W. Schulze, and F.W. Froben, *Chem. Phys. Lett.* **77**, 514 (1981).

23. A.E. Stevens, C.S. Feigerle, and W.C. Lineberger, *J. Chem. Phys.* **78**, 5420 (1983).

24. L.S. Wang, B. Niu, Y.T. Lee, and D.A. Shirley, *Chem. Phys. Lett.* **158**, 297 (1989).

25. L.S. Wang, B. Niu, Y.T. Lee, D.A. Shirley, and K. Balasubramanian, *J. Chem. Phys.* **92**, 899 (1990).

26. K.P. Huber and G. Herzberg, *Molecular Spectra and Molecular Structure. IV. Constants of Diatomic Molecules* (Van Nostrand Reinhold Co., New York, 1979).

27. K. Balasubramanian, *Chem. Phys.* **119**, 41 (1988).

28. T.Y. Cheng, K.F. Willey, J.E. Salcido, and M.A. Duncan, *Int. J. Mass Spectrom. Ion Processes*, in press, 1990.

29. M.A. Duncan, private communication.

Table 1. Experimental conditions.

	T (K)[a]	P (Torr)[b]	f (mm)[c]	Starting materials[d]
As_2	1400	350 (Ne)	0.13	Cu_3As
Sb_2	1150	600 (Ne)	0.13	Pure antimony
Bi_2	1100	500 (Ne)	0.13	Pure bismuth

a. Oven temperature (±50K).

b. Carrier gas pressure.

c. Nozzle diameter.

d. Samples were all purchased from CERAC.

Table 2. Valence Gaussian basis sets used for As, Sb, and Bi.

Atom	Orbital Type	Exponent	Contraction Coefficient
As	s	1.2210	1.0
	s	0.3200	1.0
	s	0.1138	1.0
	s	0.0405	1.0
	p	1.9760	1.0
	p	0.3232	1.0
	p	0.1024	1.0
	p	0.0324	1.0
	d	50.14	0.06133
	d	13.81	0.28264
	d	4.383	0.52548
	d	1.304	1.0
	d	0.388	1.0
	d	0.115	1.0
Sb	s	0.5598	1.0
	s	0.4423	1.0
	s	0.1121	1.0
	s	0.0288	1.0
	p	0.9967	1.0
	p	0.2405	1.0
	p	0.0814	1.0
	p	0.0276	1.0
	d	3.5213	0.299648
	d	1.6791	0.452924
	d	0.7781	0.321395
	d	0.3187	1.0
	d	0.1305	1.0
	d	0.0534	1.0
Bi	s	0.6781	1.0
	s	0.3256	1.0
	s	0.1102	1.0
	s	0.0373	1.0

Table 2. (Continued)

Atom	Orbital Type	Exponent	Contraction Coefficient
Bi	p	0.8761	1.0
	p	0.2230	1.0
	p	0.0761	1.0
	p	0.0260	1.0
	d	1.6920	0.588039
	d	0.6623	0.439133
	d	0.2589	1.0
	d	0.1011	1.0
	d	0.0395	1.0

Table 3. Spectroscopic constants for As_2 and As_2^+.[a]

		R_e (Å)		ω_e (cm^{-1})		IPa (eV)[b]		IPv (eV)[c]	D_e (eV)	
		Exp.	Theo.	Exp.	Theo.	Exp.	Theo.	Exp.	Exp.	Theo.
As_2	$^1\Sigma_g^+$	2.1026	2.16	430.0	394				3.96	3.05
As_2^+	$^2\Pi_{u3/2}$	2.230(8)	2.230	385(8)	347	9.636(6)	9.32	9.779(6)	4.11	
	$^2\Pi_{u1/2}$	2.235(8)	2.231	380(5)	347	9.810(6)	9.50	9.994(6)		
	($^2\Pi_u$)		2.23		347		9.41			3.59
	$^2\Sigma_g^+$	2.115(8)	2.14	390(8)	392	10.230(5)	9.84			
	($^4\Sigma_u^-$)		2.36		255		12.1			

a. The experimental spectroscopic constants for the neutral molecule are from Ref. 26.

b. The adiabatic ionization energy.

c. The vertical ionization energy.

Table 4. Spectroscopic constants for Sb_2 and Sb_2^+.[a]

		R_e (Å)		ω_e (cm^{-1})		IPa (eV)[b]		IPv (eV)[c]	D_e (eV)	
		Exp.	Theo.	Exp.	Theo.	Exp.	Theo.	Exp.	Exp.	Theo.
Sb_2	$^1\Sigma_g^+$	2.3415	2.58	270.0	259				3.09	2.17
Sb_2^+	$^2\Pi_{u3/2}$		2.670		226	(8.5)	8.13	(8.7)	(3.2)	
	$^2\Pi_{u1/2}$		2.663		226	(8.9)	8.53	(9.1)		
	$(^2\Pi_u)$		2.66		227		8.36			2.97
	$^2\Sigma_g^+$	2.37(1)	2.59	235(10)	223	9.275(5)	8.78			

a. The experimental spectroscopic constants for the neutral molecule are from Ref. 26.

b. The adiabatic ionization energy.

c. The vertical ionization energy.

Table 5. Spectroscopic constants for Bi_2 and Bi_2^+.[a]

	R_e (Å)		ω_e (cm^{-1})[b]		IPa (eV)[c]		IPv (eV)[d]	D_e (eV)	
	Exp.	Theo.	Exp.	Theo.	Exp.	Theo.	Exp.	Exp.	Theo.
Bi_2 $^1\Sigma_g^+(0_g^+)$	2.66	2.84	172.71	171				2.04	1.38
Bi_2^+ $^2\Pi_{u3/2}$	(2.86)	3.01	(140)	129	7.440(7)	7.26	7.623(7)	1.89	
$^2\Pi_{u1/2}$	(2.84)	3.00	(140)	134	8.865(7)	8.67	8.991(7)		
$(^2\Pi_u)$		2.98		141		8.35			
$^2\Sigma_g^+$	2.705(8)	2.99	150(8)	136	9.307(5)	8.97			

a. The experimental spectroscopic constants for the neutral molecule are from Ref. 26.

b. The experimental ω_e for Bi_2 is from Ref. 22.

c. The adiabatic ionization energy.

d. The vertical ionization energy.

Figure Captions

Figure 1 The HeI photoelectron spectrum of As_2^+. HB stands for the hot band transitions.

Figure 2 The HeI photoelectron spectrum of Sb_2^+. The $^3P_2$, $^3P_1$, and $^3P_0$ peaks shown are the subtracted atomic lines. The $^2\Pi_{u1/2}$ and $^2\Pi_{u3/2}$ bands have large contributions from Sb_4^+ $[(2t_2)^{-1}]$ bands.

Figure 3 The HeI photoelectron spectrum of Bi_2^+. The arrows indicate positions of the three subtracted atomic lines.

Figure 4 A Franck-Condon factor simulation of the $^2\Sigma_g^+$ band of As_2^+. Individual lines represent the Franck-Condon factors, each of which is convoluted with a Gaussian (width 0.027 eV) to compare with the experimental spectrum. (– calculated, ... experimental).

Figure 5 A Franck-Condon factor simulation of the $^2\Pi_{u3/2}$ band of As_2^+. Individual lines represent the Franck-Condon factors, each of which is convoluted with a Gaussian (width 0.027 eV) to compare with the experimental spectrum. (– calculated, ... experimental).

Figure 6 A Franck-Condon factor simulation of the $^2\Pi_{u1/2}$ band of As_2^+. Individual lines represent the Franck-Condon factors, each of which is convoluted with a Gaussian (width 0.027 eV) to compare with the experimental spectrum. (– calculated, ... experimental).

Figure 7 A Franck-Condon factor simulation of the $^2\Sigma_g^+$ band of Bi_2^+. Individual lines represent the Franck-Condon factors, each of which is convoluted with a Gaussian (width 0.018 eV) to compare with the experimental spectrum. (– calculated, ... experimental).

Figure 8 CASSCF/CI potential energy curves for As_2 and As_2^+.

Figure 9 CASSCF/CI/RCI potential energy curves for Sb_2 and Sb_2^+. The solid curves do not include the spin-orbit effects, and the dashed curves include the spin-orbit effects.

Figure 10 CASSCF/RCI potential energy curves for Bi_2 and Bi_2^+. The solid curves do not include the spin-orbit effects, and the dashed curves include the spin-orbit effects.

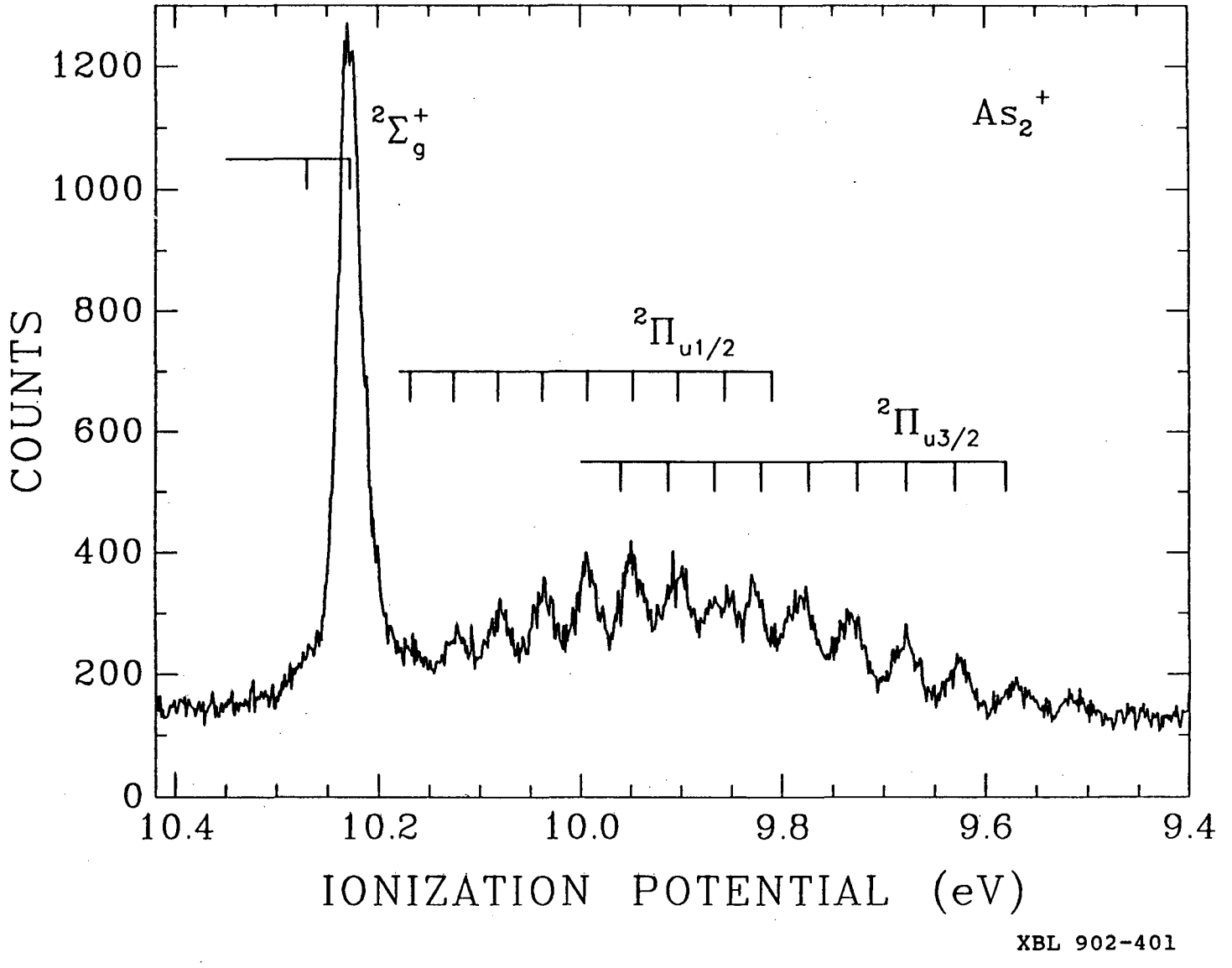
1200
1000
800
600
400
200
0
COUNTS
$^2\Sigma_g^+$
As_2^+
$^2\Pi_{u1/2}$
$^2\Pi_{u3/2}$
10.4
10.2
10.0
9.8
9.6
9.4
IONIZATION POTENTIAL (eV)
XBL 902-401

Figure 1

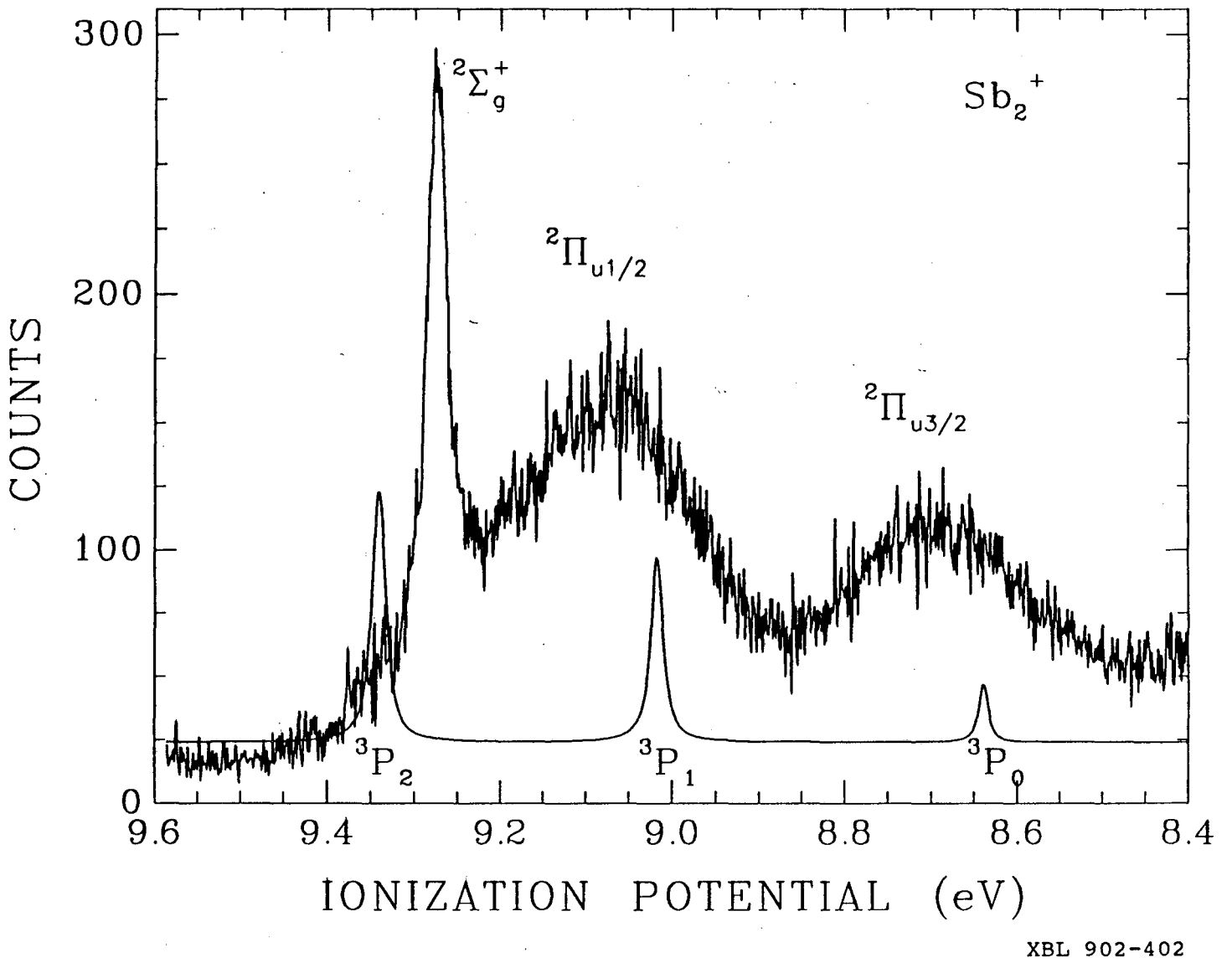
300
200
100
0
COUNTS
$^2\Sigma_g^+$
Sb_2^+
$^2\Pi_{u1/2}$
$^2\Pi_{u3/2}$
$^3P_2$
$^3P_1$
$^3P_0$
9.6
9.4
9.2
9.0
8.8
8.6
8.4
IONIZATION POTENTIAL (eV)
XBL 902-402

Figure 2

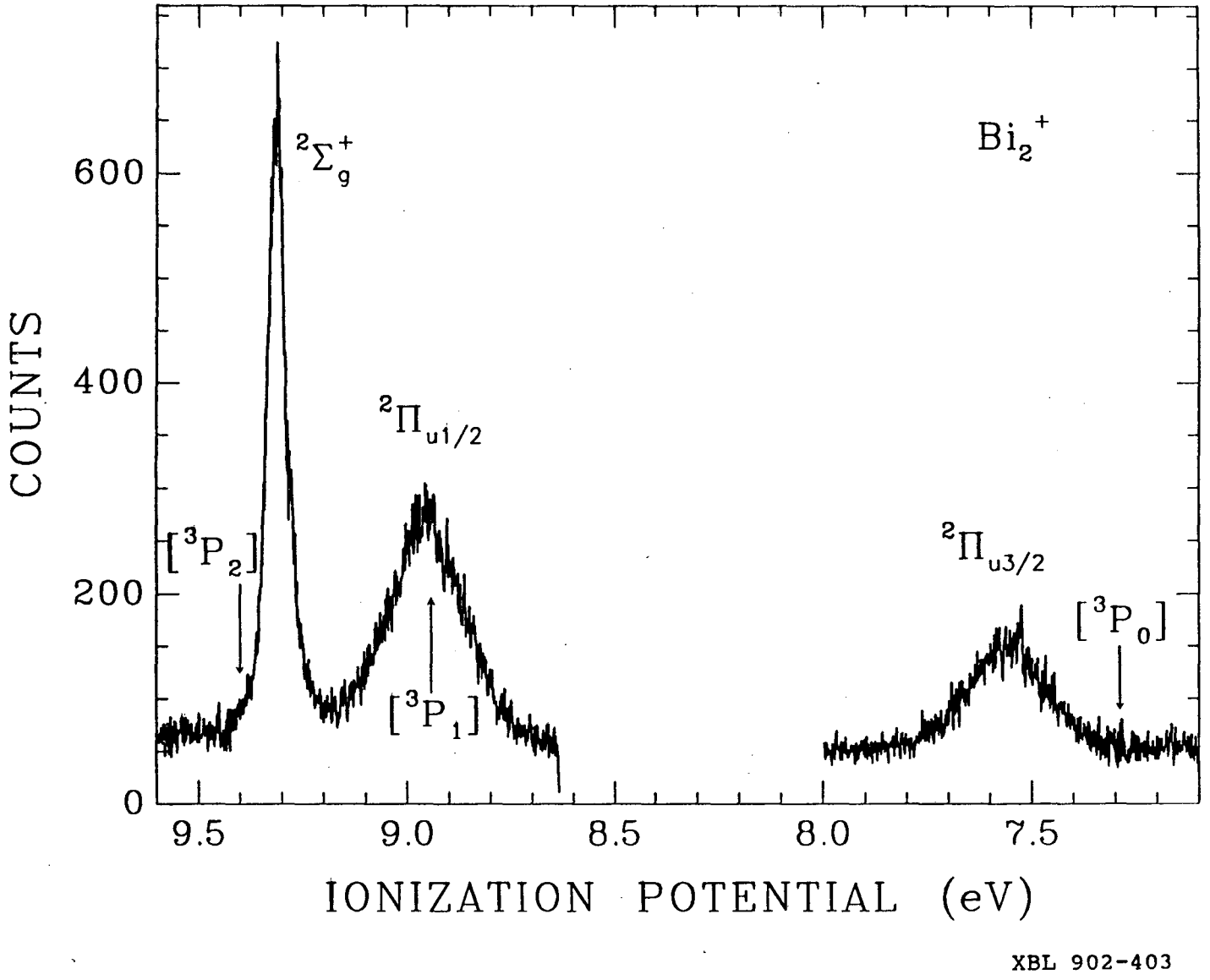
COUNTS
600
400
200
0
$^2\Sigma_g^+$
Bi_2^+
$^2\Pi_{u1/2}$
$^2\Pi_{u3/2}$
$[^3P_2]$
$[^3P_1]$
$[^3P_0]$
9.5
9.0
8.5
8.0
7.5
IONIZATION POTENTIAL (eV)
XBL 902-403

Figure 3

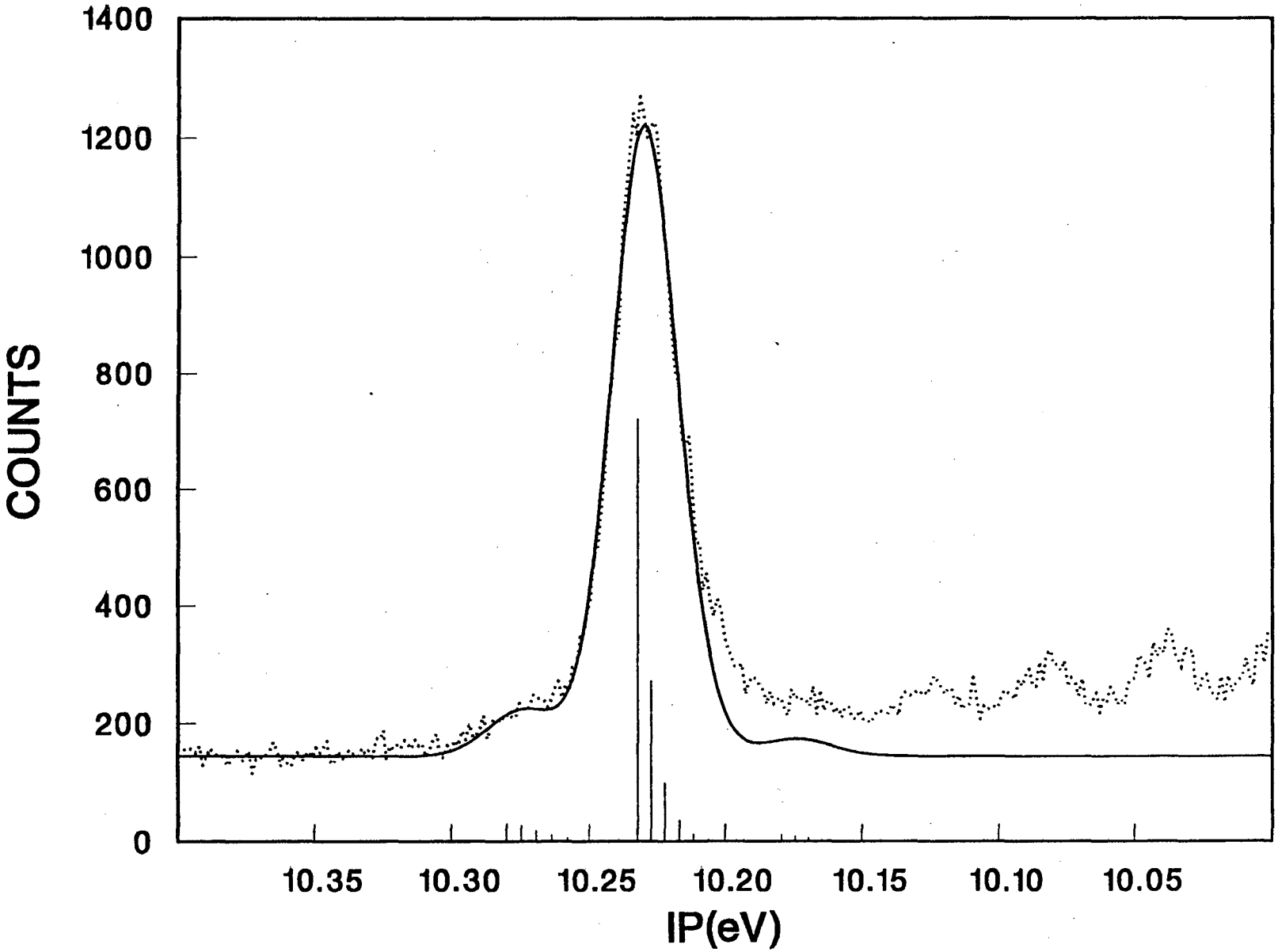
1400
1200
1000
800
600
400
200
0
COUNTS
10.35
10.30
10.25
10.20
10.15
10.10
10.05
IP(eV)

Figure 4

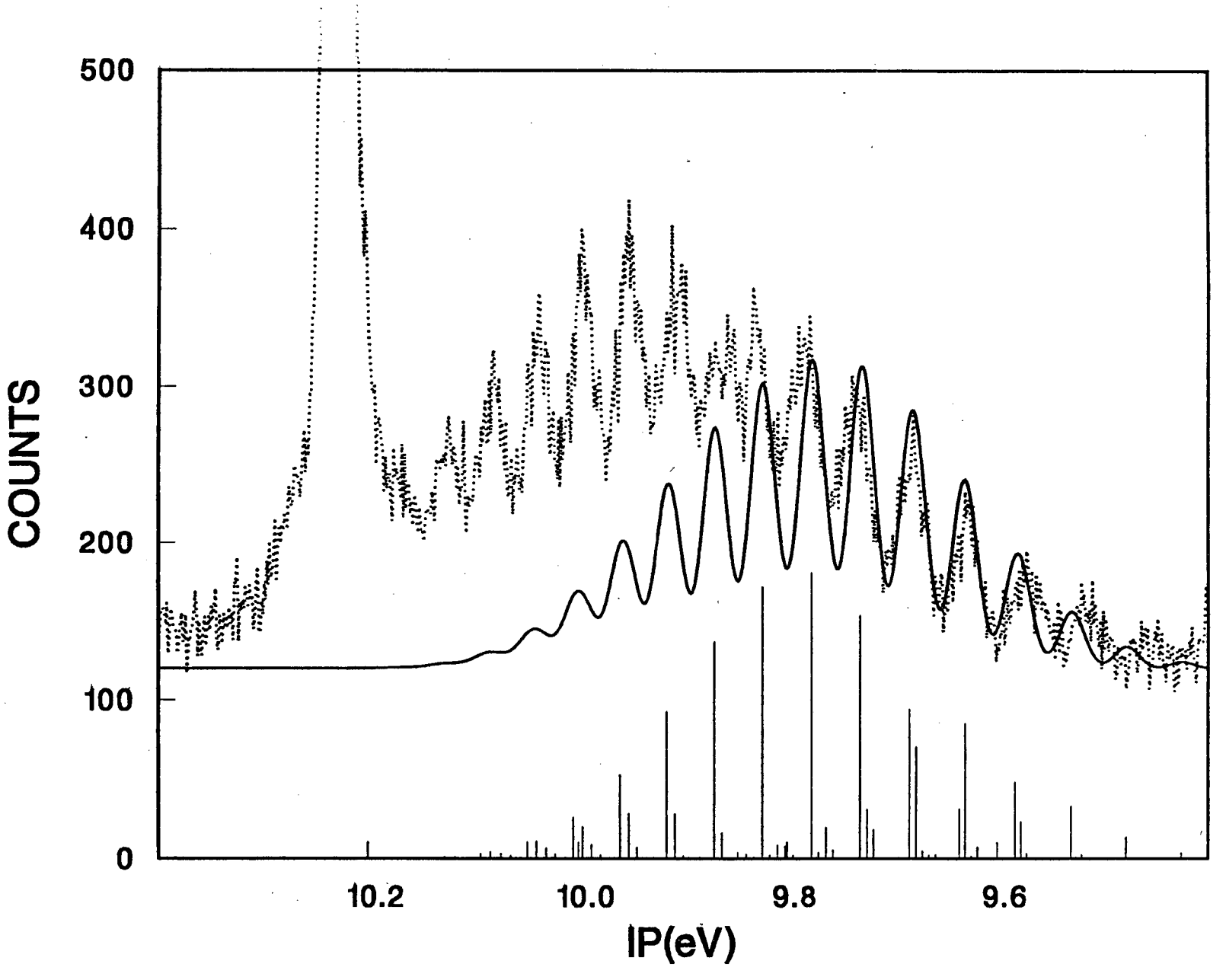

Figure 5

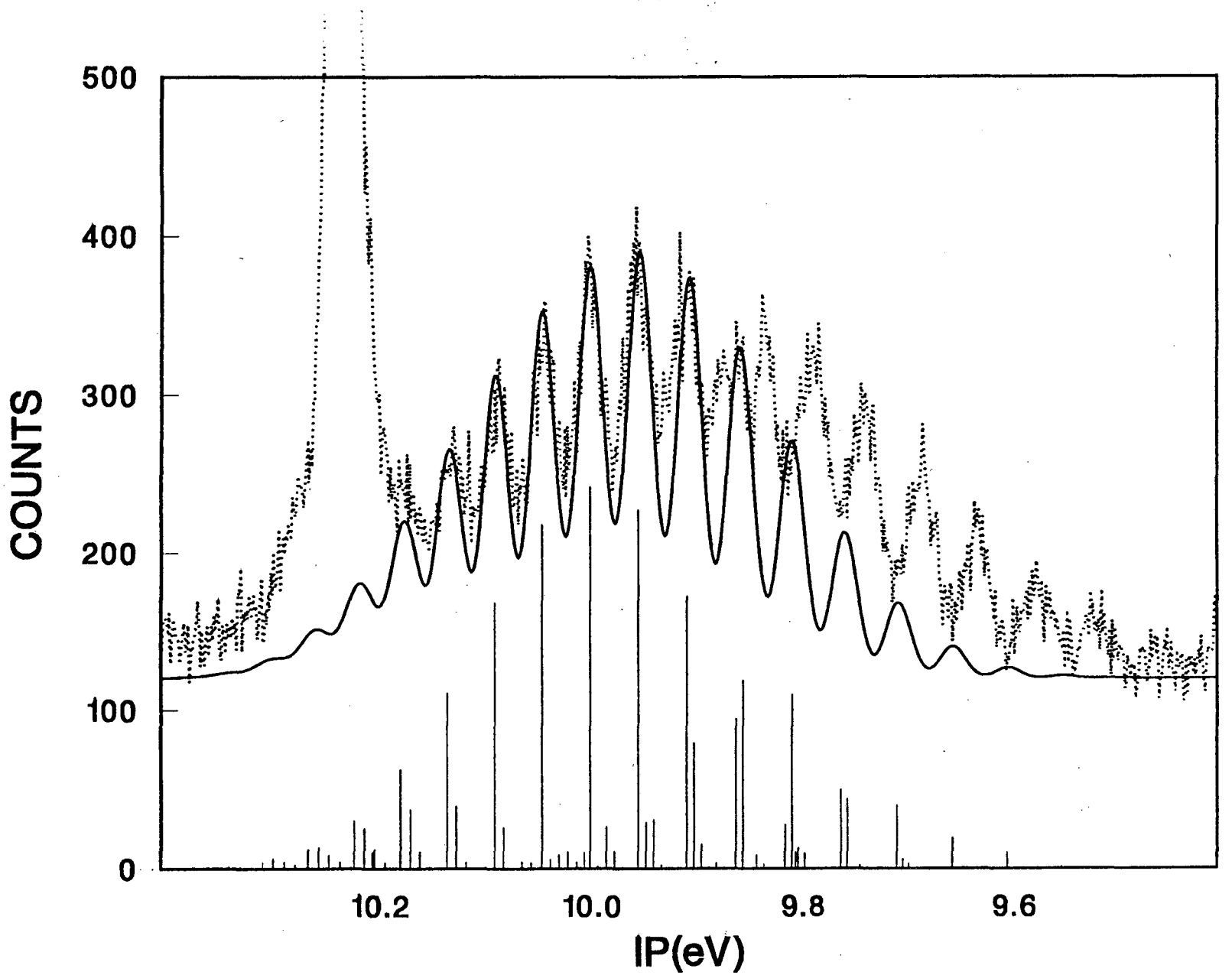

Figure 6

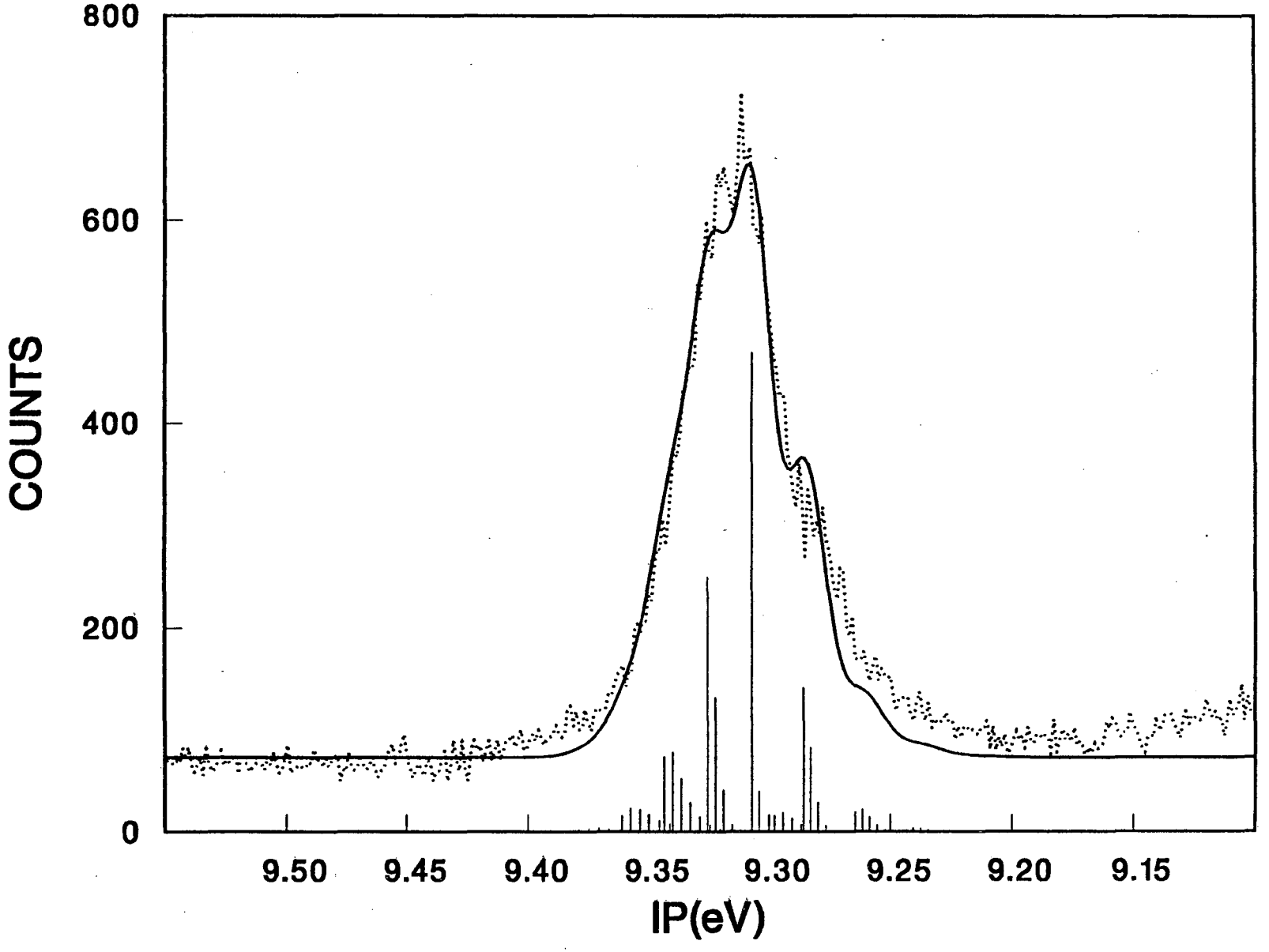

Figure 7

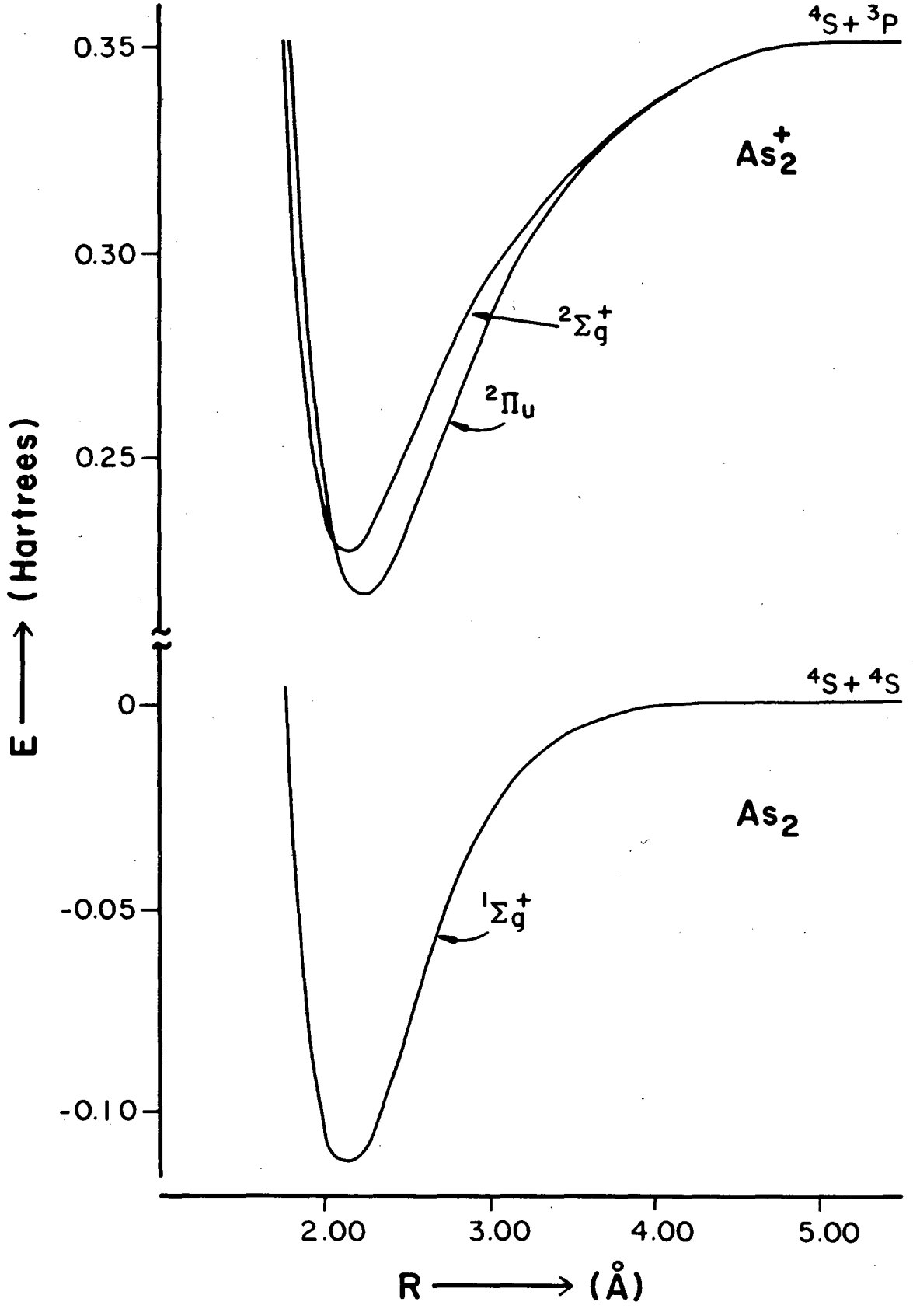
$^4S + {}^3P$
0.35
0.30
0.25
As_2^+
$^2\Sigma_g^+$
$^2\Pi_u$
E ⟶ (Hartrees)
$^4S + {}^4S$
0
-0.05
-0.10
As_2
$^1\Sigma_g^+$
2.00
3.00
4.00
5.00
R ⟶ (Å)

Figure 8

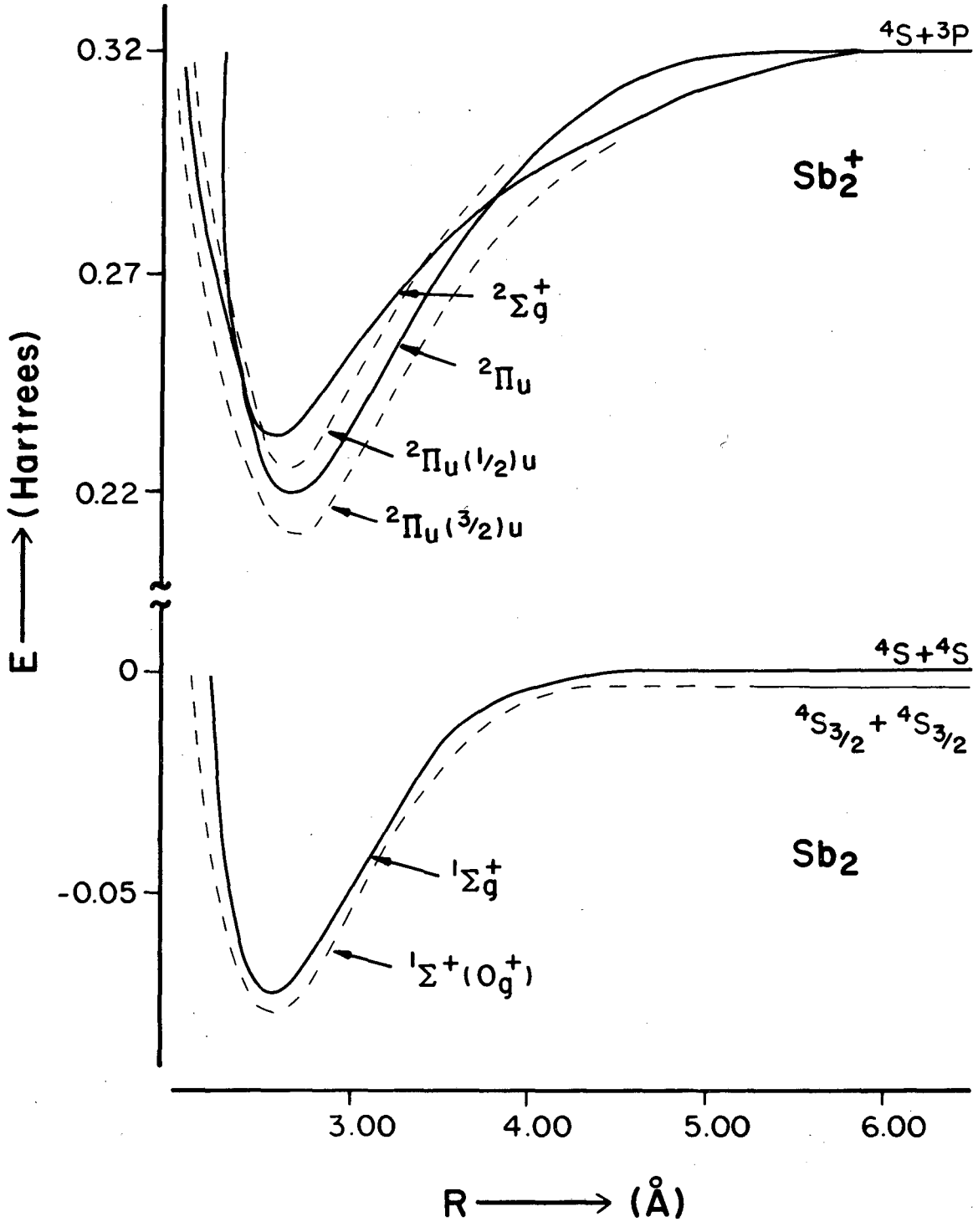
0.32
0.27
0.22
0
-0.05
E ⟶ (Hartrees)
4S+3P
Sb2+
2Σg+
2Πu
2Πu(1/2)u
2Πu(3/2)u
4S+4S
4S3/2 + 4S3/2
Sb2
1Σg+
1Σ+(0g+)
3.00
4.00
5.00
6.00
R ⟶ (Å)

Figure 9

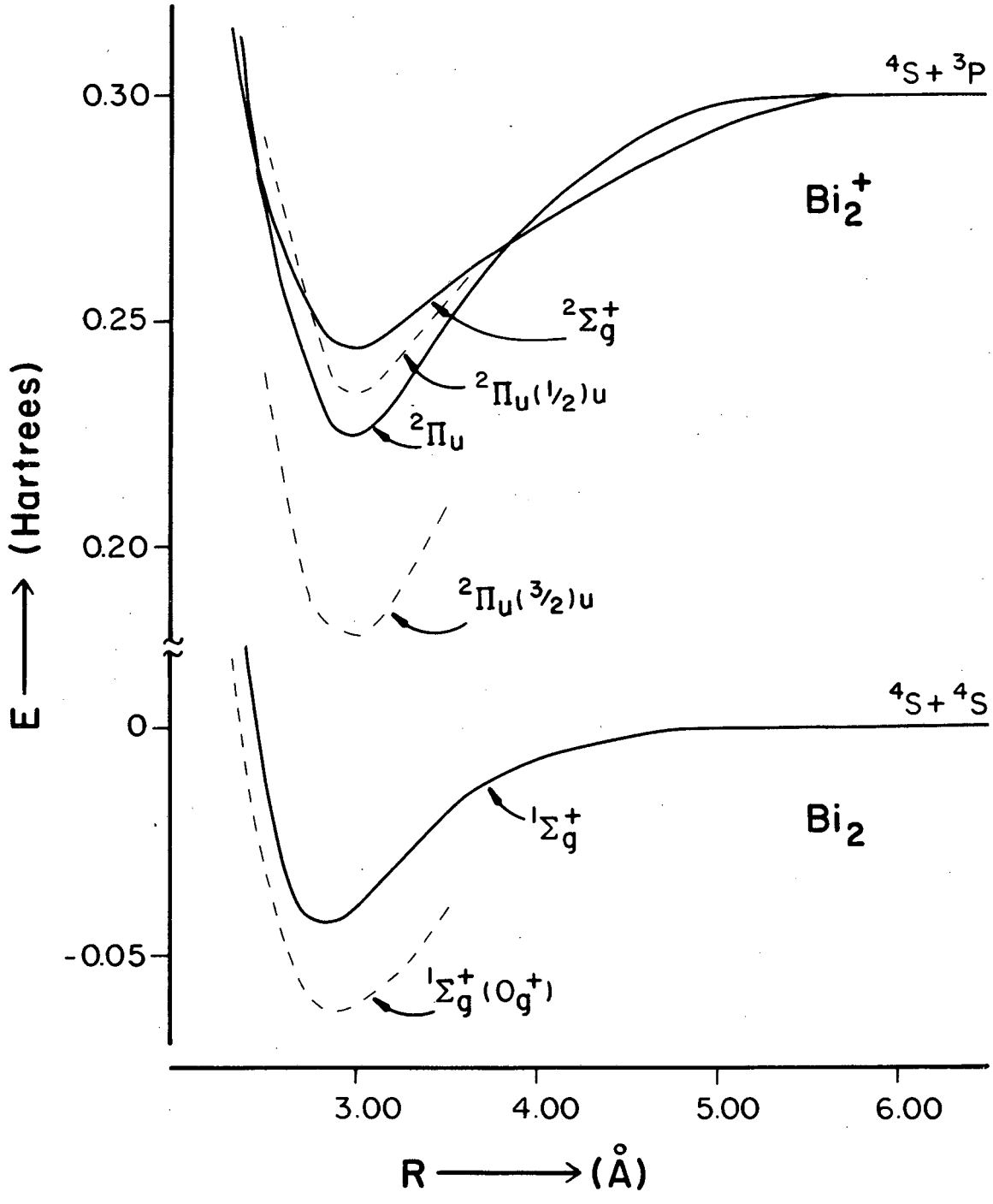
0.30
0.25
0.20
0
-0.05
E ⟶ (Hartrees)
$^4S + ^3P$
Bi_2^+
$^2\Sigma_g^+$
$^2\Pi_u(1/2)u$
$^2\Pi_u$
$^2\Pi_u(3/2)u$
$^4S + ^4S$
$^1\Sigma_g^+$
Bi_2
$^1\Sigma_g^+(0_g^+)$
3.00
4.00
5.00
6.00
R ⟶ (Å)

Figure 10

LAWRENCE BERKELEY LABORATORY
UNIVERSITY OF CALIFORNIA
INFORMATION RESOURCES DEPARTMENT
BERKELEY, CALIFORNIA 94720